HHS Public Access

Author manuscript

ACS Nano. Author manuscript; available in PMC 2017 January 10.

Published in final edited form as:

ACS Nano. 2015 December 22; 9(12): 12344–12348. doi:10.1021/acsnano.5b05629.

Photoacoustic and Colorimetric Visualization of Latent Fingerprints

Kai Song[†,§,#], **Peng Huang**[‡,⊥,*,#], **Chenglin Yi**[§], **Bo Ning**, **Song Hu**[‖], **Liming Nie**[⊥], **Xiaoyuan Chen**[⊥,*], and **Zhihong Nie**[§,*]

[†]School of Life Science, Changchun Normal University, Changchun 130032, China

[‡]Guangdong Key Laboratory for Biomedical Measurements and Ultrasound Imaging, Department of Biomedical Engineering, School of Medicine, Shenzhen University, Shenzhen 518060, China

[§]Department of Chemistry and Biochemistry, University of Maryland, College Park, Maryland 20742, United States

[‖]Department of Biomedical Engineering, University of Virginia, Charlottesville, Virginia 22903, United States

[⊥]Laboratory of Molecular Imaging and Nanomedicine (LOMIN), National Institute of Biomedical Imaging and Bioengineering (NIBIB), National Institutes of Health, Bethesda, Maryland 20892, United States

Abstract

There is a high demand on a simple, rapid, accurate, user-friendly, cost-effective, and nondestructive universal method for latent finger-print (LFP) detection. Herein, we describe a combination imaging strategy for LFP visualization with high resolution using poly(styrene-*alt*-maleic anhydride)-*b*-polystyrene (PSMA-*b*-PS) functionalized gold nanoparticles (GNPs). This general approach integrates the merits of both colorimetric imaging and photoacoustic imaging. In comparison with the previous methods, our strategy is single-step and does not require the signal amplification by silver staining. The PSMA-*b*-PS functionalized GNPs have good stability, tunable color, and high affinity for universal secretions (proteins/polypeptides/amino acids), which makes our approach general and flexible for visualizing LFPs on different substrates (presumably with different colors) and from different people. Moreover, the unique optical property of GNPs enables the photoacoustic imaging of GNPs-deposited LFPs with high resolution. This allows observation of level 3 hyperfine features of LFPs such as the pores and ridge contours by photoacoustic imaging. This technique can potentially be used to identify chemicals within LFP residues. We believe that this dual-modality imaging of LFPs will find widespread use in forensic investigations and medical diagnostics.

[*]Address correspondence to peng.huang@nih.gov, shawn.chen@nih.gov, znie@umd.edu.
[#]The authors K.S. and P.H. equally contributed to this article.

Conflict of Interest: The authors declare no competing financial interest.

Supporting Information Available: The Supporting Information is available free of charge on the ACS Publications website at DOI: 10.1021/acsnano.5b05629.
More experimental information, discussions and data (PDF)

Graphical Abstract

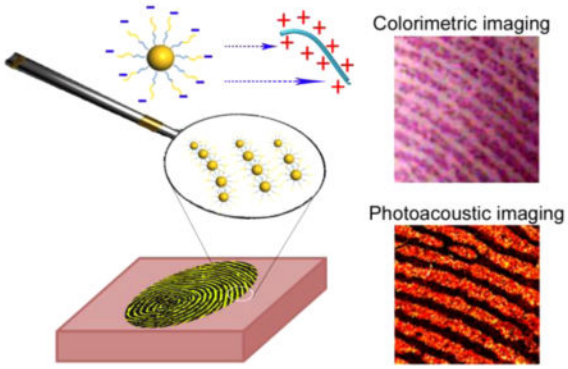

Keywords

latent fingerprints; colorimetric imaging; photoacoustic imaging; block copolymer; gold nanoparticles

Fingerprints (FPs) with unique patterns have been used as important physical evidence in forensic investigations to identify individuals since the late 19th century.[1,2] In the past decade, with the development of human intelligence, more information about an individual can be obtained by detecting the residues of various chemicals and metabolites in FPs, thus identifying drugs ingested, and explosives or drugs handled by a person.[3–7] However, in many cases, FPs are invisible to the naked eye, known as latent fingerprints (LFPs).[8,9] Over the last century, there have been numerous techniques explored for the visualization of LFPs.[4] Although many of them have been used successfully at the scene of a crime for forensic investigations, there is still a high demand for a simple, rapid, accurate, user-friendly, cost-effective, and nondestructive universal method for LFP detection.[4]

The basic principle of LFP detection is the enhancement of optical contrast between the ridges of the FP and the support substrate.[10] Due to their fascinating physicochemical properties, inorganic nano-particles have been widely employed for LFP detection,[11] such as gold nanoparticles (GNPs),[3,12] magnetic nanoparticles,[2] semiconductor quantum dots (QDs),[13,14] upconversion nanoparticles (UCNPs),[10] *etc.* Stable GNPs have attracted increasing attention for improving optical contrast in LFP detection. For example, multimetal deposition (MMD) is a well-known technique with high sensitivity for visualizing LFPs on both porous and nonporous surfaces, which involves the deposition of GNPs on finger secretions followed by silver staining for signal amplification.[15,16] Recently, Su *et al.* reported an immunological multimetal deposition (iMMD) that combines the conventional MMD with the immunoassay technique.[17] Although MMD has many advantages, it still suffers from several drawbacks, including labor intensiveness, poor accuracy, and flat-colored (only gray or black) images.[3] Moreover, MMD can only visualize LFPs, and is not applicable to the detection of analytes of interest in LFPs.[18]

Herein, we report a simple, one-step, rapid, and nondestructive universal strategy for visualizing LFPs by using amphiphilic block copolymer (BCP) poly-(styrene-*alt*-maleic

anhydride)-*b*-polystyrene (PSMA-*b*-PS) functionalized GNPs (Figure 1). The as-prepared GNPs specifically interact with universal secretions (proteins/polypeptides/amino acids) in the fingerprint residues through both electrostatic and hydrophobic interactions.[15] This approach can be applied to visualize LFPs on different surfaces and from different people. By controlling the level of 1-dodecanethiol-induced self-assembly of as-prepared GNPs, the colorimetric image of LFPs was successfully recognized with the naked eye. To obtain high resolution images of LFPs, photoacoustic imaging was applied to observe the hyperfine structures of LFPs such as the pores and ridge contours (level 3 features).

RESULTS AND DISCUSSION

The amphiphilic BCP of dithioester-terminated $PSMA_{12}$-*b*-PS_{18} was synthesized using a previously reported method[19] (Figure S1 and S2). The PSMA-*b*-PS chains were covalently grafted onto the surface of GNPs with a diameter of ~30 nm *via* gold–thiol bond. The functionalized spherical GNPs show high dispersibility and good stability in aqueous solution (Figure S3), due to the negative charges on the surface of GNPs (the value of zeta potential is −42 ± 5.2 mV). The localized surface plasmon resonance (LSPR) peak of the BCP-grafted GNPs is located at 520 nm, which is similar to that of original GNPs (Figure S3).

The BCP functionalized GNPs for LFP visualization was tested by immersing the fingerprint sample in an aqueous PSMA-*b*-PS-grafted GNPs solution of pH 2.5–2.8 for 30–45 min incubation. If the incubation time is over 1 h, it may cause some deposition due to the spreading of compounds. Under this acidic condition, proteins/polypeptides/amino acids within LFP residues are protonated and thus exhibit positive charges.[15] Meanwhile, the PSMA-*b*-PS polymer is easy to hydrolyze to produce numerous carboxylate groups, which makes the GNPs negatively charged. Because of the electrostatic attraction between opposite charges, GNPs are deposited preferentially on the LFP ridges. In addition, the hydrophobic interactions between PS block of the BCP and hydrophobic regions on protein surfaces can promote the selective adsorption of GNPs on the LFPs. We thus suggest the strong binding of GNPs and LFPs residues is a result of both electrostatic and hydrophobic interactions. After GNP deposition, the LFP image clearly showed the typical fingerprint ridge pattern with sufficient details that would enable an individual to be identified (Figure S4).

The applicability of BCP functionalized GNPs in LFP visualization was investigated on three typical surfaces: porous (paper, paper money), semiporous (plastic tape, plastic), and nonporous (silicon wafer, glass) surfaces. As shown in Figure 2, the ridge pattern details of LFPs from different people on all tested surfaces could be easily recognized by naked eyes, which would provide clear evidence for individual identification. These results suggest that this strategy can be utilized successfully to visualize LFPs on different substrates and from different people, clearly demonstrating good generalizability of this approach.

For LFP visualization, the enhancement of optical contrast between the ridges of the FP and the support substrate is most important to examine with naked eyes. As LFPs might be present on support substrates with different colors, successful colorimetric imaging requires recognition of LFPs without background interference. The association of GNPs in the

presence of 1-dodecanethiol leads to the interparticle plasmonic coupling and color change of GNP solution from red to dark blue (Figure 3a). LFPs treated with BCP functionalized GNPs at different self-assembly levels show different colors (Figure 3b). The obvious red-shift in extinction spectra upon self-assembly was observed in the UV–visible spectra in Figure 3c.[20,21] The self-assembly of BCP functionalized GNPs was also evidenced by SEM images (Figure 3d). The size of aggregates increased with increasing amount of 1-dodecanethiol in the GNP solution. We also obtained similar results using PSMA-*b*-PS functionalized gold nanorods (GNRs) for enhanced LFPs visualization (Figure S5), which suggests that this colorimetric imaging strategy of LFPs can be extended to other plasmonic nanoparticles with different shapes.

The colorimetric imaging of LFPs using PSMA-*b*-PS functionalized GNPs can be easily recognized with the bare eye, which would provide clear evidence for individual identification. However, second level (ridge bifurcations, terminations, and crossovers) and third level (pores and ridge contours) details are hard to be distinguished. The LSPR of PSMA-*b*-PS functionalized GNPs shows great potential for photoacoustic imaging (PAI), due to its high intensity, nonblinking, and optical stability.[22–24] In addition, since the PAI amplitude is proportional to optical absorption, PAI can be used to detect the optical absorption of LFP with high sensitivity.[25] It is not surprising that the second and third level details of LFP cannot be recognized under normal optical microscopy (Figure 4a). The PAI of LFP was tested by using a well-established optical-resolution photoacoustic microscope[25,26] (Figure S6). Second and third level details could be clearly distinguished in Figure 4b,c. The enhancement of LFP can be semiquantitatively confirmed by PAI amplitude. As shown in Figure 4d,e, the PA amplitudes vary significantly from ridge to furrow.

In this strategy, PSMA-*b*-PS can be replaced by other biomolecules such as antibodies, aptamers, and so on for the detection of specific LFP residues, such as illicit drugs, and explosives. Through molecular recognitions, the chemical compositions of target species within LFP residues can be potentially identified/differentiated based on the optical contrast and amplitude of PAI images.[25] As a result, the colorimetric imaging can give clear and high-quality images of fingerprints for individual identification by bare eyes, while simultaneous PAI can be applied to observing hyperfine resolution and detecting the residues of various chemicals and metabolites, thus showing great potential in forensic investigation.

CONCLUSION

In summary, we report a combination imaging strategy for LFP visualization with high resolution. This general approach integrates the merits of both colorimetric imaging and photoacoustic imaging. In comparison with the previous methods, our strategy is single-step and does not require signal amplification by silver staining. The PSMA-*b*-PS functionalized GNPs have high dispersibility, good stability, tunable color, and high affinity with universal secretions (proteins/polypeptides/amino acids), which makes our approach general and flexible for visualizing LFPs on different substrates (presumably with different colors) and from different people. Moreover, the unique optical property of GNPs enables the PAI of

GNPs-deposited LFPs with high resolution. To the best of our knowledge, this is the first report of PAI observation of level 3 hyperfine structures of LFPs such as the pores and ridge contours. This PAI technique can potentially be used to identify chemicals within LFP residues. We believe that this dual-modality imaging of LFPs will find widespread use in forensic investigations and medical diagnostics.

EXPERIMENTAL SECTION

Synthesis of BCP PSMA-*b*-PS

Maleic anhydride (MA) and styrene (St), forming charge transfer complex (CTC) monomer pairs, can be alternately polymerized *via* free radical initiating techniques. With the use of RAFT polymerization method, excess styrene will continue to grow into a second block to produce diblock copolymers after CTC monomer pairs have been consumed in the polymerization of the first alternating block.[19]

Briefly, dithioester-terminated PSMA-*b*-PS was synthesized *via* RAFT polymerization method. The synthetic procedure is shown in Figure S1a. CPDB (0.09 g, 0.4 mmol), styrene (4.77 g, 45 mmol), MA (0.49 g, 5 mmol), and AIBN (16 mg, 0.1 mmol) were dissolved in 10 mL of dioxane in a 25 mL flask. The reaction mixture was degassed under vacuum for 30 min and refilled with nitrogen for three times. The flask was then placed in a preheated oil bath at 65 °C for 18 h. After polymerization, the polymer was obtained by precipitating in diethyl ether three times and dried under vacuum overnight. From the ^{1}H NMR spectrum (in DMSO-d_6, Figure S2), the NMR-based M_w (NMR) is 4.6 kg/mol, by comparing the integrals of the resonance peaks of aromatic ring in CPDB (7.4–7.9 ppm), the integrals of the resonance peaks of aromatic ring of styrene unit (6.4–7.3 ppm), and the integrals of the resonance peaks of –CH– of maleic anhydride unit (3.2–3.4 ppm). The first block, poly(styrene-*alt*-maleic anhydride) PSMA with alternating sequence was subsequently converted into highly hydrophilic and negatively charged block, poly(styrene-*alt*-maleic acid) through hydrolysis reaction (Figure S1b).

Preparation of the PSMA-*b*-PS Tethered GNPs Aqueous Solution

A 2.5 mg of BCPs was first dissolved in 5 mL of DMF. Then, a concentrated DMF solution of GNPs (~2 mg/mL, 5 mg AuNPs) was added dropwise into the above solution under vigorous shaking. Subsequently, the mixture was sonicated for 1 h and then incubated overnight to allow ligand exchange. The BCPs tethered GNPs were purified by centrifugation 3 times and redispersed in DMF with a concentration of around 1.0 mg/mL. Volumes of 0.5 mL triethylamine and 0.1 mL water were added into the DMF solution of BCPs tethered GNPs under stirring. About 2 h later, 5.0 mL of triethylamine and 1.0 mL of water were dropwisely added into the solution and then kept for one more hour. The first block of the PSMA-*b*-PS on the surface of GNPs was hydrolyzed during this process (Figure S1b). Finally, the BCPs tethered GNPs were transferred into pure water by centrifugation and redispersed in water with a concentration of around 0.5 mg/mL. The pH value of BCPs tethered GNPs aqueous solution was finally adjusted to 2.5–2.8 with citric acid (1 M).

Self-Assembly of PSMA-*b*-PS Tethered GNPs by 1-Dodecanethiol

Before adjusting the pH value, predetermined amount of 1-dodecanethiol (1, 2, 4, 6, 8, 10 μL) was added into the BCPs tethered GNPs aqueous solution. The mixture was incubated for 8 h and purified by centrifugation 3 times. The self-assembly of PSMA-*b*-PS tethered GNPs was redispersed in water. Then, the pH value of the solution was adjusted to 2.5–2.8 by the above method.

Latent Fingerprints (LFPs) Visualization

The latent fingerprints (LFPs) were immersed in an aqueous PSMA-*b*-PS-grafted GNPs solution (0.5 mg/mL) of pH 2.5–2.8 for 30–45 min. The LFPs were then dried for further colorimetric and photoacoustic imaging. The same method was used for 1-dodecanethiol induced self-assembly of PSMA-*b*-PS tethered GNPs system.

Photoacoustic Imaging of LFPs

The performance of the sample for microscope-level LFPs imaging was tested by using a well-established optical-resolution photoacoustic microscope (PAM).[25,26] In the PAM system, a high-speed fast nanosecond-pulsed laser (Edgewave, BX40-2) with 532 nm wavelength was applied for illumination. The laser output beam was attenuated by a neutral-density filter (Thorlabs, NDC-50C-2M), and reduced to the same diameter by an iris (Thorlabs, SM1D12D) for fiber-optic coupling. A condenser lens (Thorlabs, LA1608) and 50-μm-diameter pinhole (Thorlabs, P50C) were used to a reshaped the beam before it was coupled into a single-mode optical fiber (Thorlabs, P1-460B-FC-2) through a microscope objective (Newport, M-10X). Approximately 5% of the laser energy was tapped off by a beam sampler (Thorlabs, BSF10-A) for monitoring laser intensity fluctuations. At the scan head, the laser beams were collimated and focused into the object to be imaged through two doublets (Thorlabs, AC127-025-A), providing a lateral resolution of ~2.7 μm. A 2D galvanometer scanner (Cambridge, 6215HSM40B) was inserted to align the optical and acoustic foci to the confocal position. An iris (Thorlabs, SM05D5) was used to match the beam with the dimension of the galvo mirrors. Finally, a ring transducer which allows the beam to path through was applied to detect the generated photoacoustic signals from the GNPs, and the signals were digitally acquired with a 500 MHz sampling rate. The used laser pulse energy was 6 nJ, with a repetition rate of 10 kHz. Conventional raster scan was performed to image a 12 mm × 12 mm big LFPs area, with step sizes of 5 and 1.67 μm between successive B-scans and A-lines, respectively.

Supplementary Material

Refer to Web version on PubMed Central for supplementary material.

Acknowledgments

This work was supported by the startup funds from the Shenzhen University and University of Maryland, the National Natural Science Foundation of China (81401465, 51573096, 11204021, 81272987), the National Science Foundation (CHE-1505839) and the Intramural Research Program (IRP) of the NIBIB/NIH.

REFERENCES AND NOTES

1. Almog J, Hirshfeld A, Klug JT. Reagents for the Chemical Development of Latent Fingerprints: Synthesis and Properties of Some Ninhydrin Analogues. J Forensic Sci. 1982; 27:912–917. [PubMed: 7175471]
2. Hazarika P, Jickells SM, Wolff K, Russell DA. Imaging of Latent Fingerprints through the Detection of Drugs and Metabolites. Angew Chem, Int Ed. 2008; 47:10167–10170.
3. Li K, Qin W, Li F, Zhao X, Jiang B, Wang K, Deng S, Fan C, Li D. Nanoplasmonic Imaging of Latent Fingerprints and Identification of Cocaine. Angew Chem, Int Ed. 2013; 52:11542–11545.
4. Hazarika P, Russell DA. Advances in Fingerprint Analysis. Angew Chem, Int Ed. 2012; 51:3524–3531.
5. Wood M, Maynard P, Spindler X, Lennard C, Roux C. Visualization of Latent Fingermarks Using an Aptamer-Based Reagent. Angew Chem, Int Ed. 2012; 51:12272–12274.
6. Ifa DR, Manicke NE, Dill AL, Cooks RG. Latent Fingerprint Chemical Imaging by Mass Spectrometry. Science. 2008; 321:805. [PubMed: 18687956]
7. Wolfbeis OS. Nanoparticle-Enhanced Fluorescence Imaging of Latent Fingerprints Reveals Drug Abuse. Angew Chem, Int Ed. 2009; 48:2268–2269.
8. Tan J, Xu L, Li T, Su B, Wu J. Image-Contrast Technology Based on the Electrochemiluminescence of Porous Silicon and Its Application in Fingerprint Visualization. Angew Chem, Int Ed. 2014; 53:9822–9826.
9. Xu L, Li Y, Wu S, Liu X, Su B. Imaging Latent Fingerprints by Electrochemiluminescence. Angew Chem, Int Ed. 2012; 51:8068–8072.
10. Wang J, Wei T, Li X, Zhang B, Wang J, Huang C, Yuan Q. Near-Infrared-Light-Mediated Imaging of Latent Fingerprints Based on Molecular Recognition. Angew Chem, Int Ed. 2014; 53:1616–1620.
11. Sametband M, Shweky I, Banin U, Mandler D, Almog J. Application of Nanoparticles for the Enhancement of Latent Fingerprints. Chem Commun (Cambridge, U K). 2007:1142–1144.
12. Leggett R, Lee-Smith EE, Jickells SM, Russell DA. "Intelligent" Fingerprinting: Simultaneous Identification of Drug Metabolites and Individuals by Using Antibody-Functionalized Nanoparticles. Angew Chem, Int Ed. 2007; 46:4100–4103.
13. Menzel ER, Savoy SM, Ulvick SJ, Cheng KH, Murdock RH, Sudduth MR. Photoluminescent Semiconductor Nanocrystals for Fingerprint Detection. J Forensic Sci. 2000; 45:545–551. [PubMed: 10855957]
14. Jin YJ, Luo YJ, Li GP, Li J, Wang YF, Yang RQ, Lu WT. Application of Photoluminescent Cds/Pamam Nano-composites in Fingerprint Detection. Forensic Sci Int. 2008; 179:34–38. [PubMed: 18513904]
15. Choi MJ, McDonagh AM, Maynard P, Roux C. Metal-Containing Nanoparticles and Nano-Structured Particles in Fingermark Detection. Forensic Sci Int. 2008; 179:87–97. [PubMed: 18565707]
16. Becue A, Champod C, Margot P. Use of Gold Nano-particles as Molecular Intermediates for the Detection of Fingermarks. Forensic Sci Int. 2007; 168:169–176. [PubMed: 16920302]
17. He Y, Xu L, Zhu Y, Wei Q, Zhang M, Su B. Immunological Multimetal Deposition for Rapid Visualization of Sweat Fingerprints. Angew Chem, Int Ed. 2014; 53:12609–12612.
18. Spindler X, Hofstetter O, McDonagh AM, Roux C, Lennard C. Enhancement of Latent Fingermarks on Non-Porous Surfaces Using Anti-L-Amino Acid Antibodies Conjugated to Gold Nanoparticles. Chem Commun (Cambridge, U K). 2011; 47:5602–5604.
19. Zhu MQ, Wei LH, Li M, Jiang L, Du FS, Li ZC, Li FM. A Unique Synthesis of a Well-Defined Block Copolymer Having Alternating Segments Constituted by Maleic Anhydride and Styrene and the Self-Assembly Aggregating Behavior Thereof. Chem Commun. 2001:365–366.
20. Huang P, Lin J, Li W, Rong P, Wang Z, Wang S, Wang X, Sun X, Aronova M, Niu G, et al. Biodegradable Gold Nanovesicles with an Ultrastrong Plasmonic Coupling Effect for Photoacoustic Imaging and Photothermal Therapy. Angew Chem, Int Ed. 2013; 52:13958–13964.

21. Lin J, Wang S, Huang P, Wang Z, Chen S, Niu G, Li W, He J, Cui D, Lu G, et al. Photosensitizer-Loaded Gold Vesicles with Strong Plasmonic Coupling Effect for Imaging-Guided Photothermal/Photodynamic Therapy. ACS Nano. 2013; 7:5320–5329. [PubMed: 23721576]
22. Nie L, Chen X. Structural and Functional Photoacoustic Molecular Tomography Aided by Emerging Contrast Agents. Chem Soc Rev. 2014; 43:7132–7170. [PubMed: 24967718]
23. Huang P, Rong P, Lin J, Li W, Yan X, Zhang MG, Nie L, Niu G, Lu J, Wang W, et al. Triphase Interface Synthesis of Plasmonic Gold Bellflowers as near-Infrared Light Mediated Acoustic and Thermal Theranostics. J Am Chem Soc. 2014; 136:8307–8313. [PubMed: 24842342]
24. Li W, Chen X. Gold Nanoparticles for Photoacoustic Imaging. Nanomedicine (London, U K). 2015; 10:299–320.
25. Wang LV, Hu S. Photoacoustic Tomography: *In Vivo* Imaging from Organelles to Organs. Science. 2012; 335:1458–1462. [PubMed: 22442475]
26. Ning B, Kennedy MJ, Dixon AJ, Sun N, Cao R, Soetikno BT, Chen R, Zhou Q, Kirk Shung K, Hossack JA, et al. Simultaneous Photoacoustic Microscopy of Microvascular Anatomy, Oxygen Saturation, and Blood Flow. Opt Lett. 2015; 40:910–913. [PubMed: 25768144]

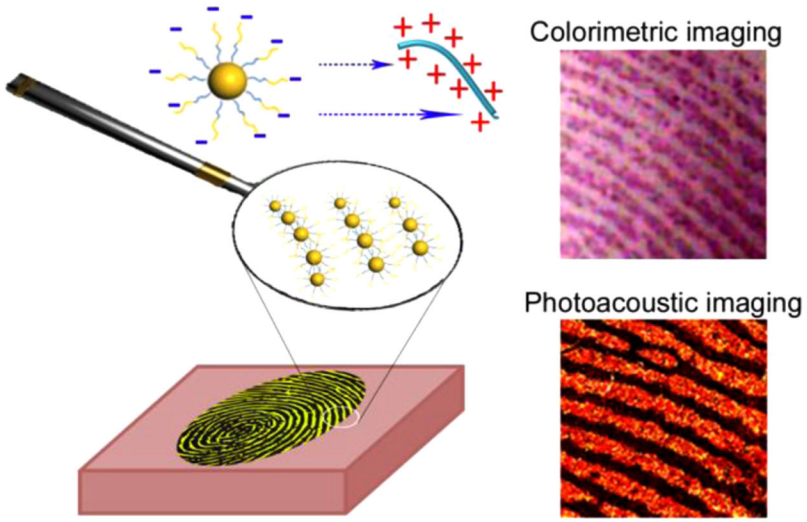

Figure 1.

Photoacoustic and colorimetric imaging of latent fingerprints (LFPs) by using amphiphilic block copolymer (BCP) poly(styrene-*alt*-maleic anhydride)-*b*-polystyrene (PSMA-*b*-PS) functionalized gold nanoparticles (GNPs). Negatively charged GNPs are preferentially attached on the LFP ridges through both electrostatic and hydrophobic interactions.

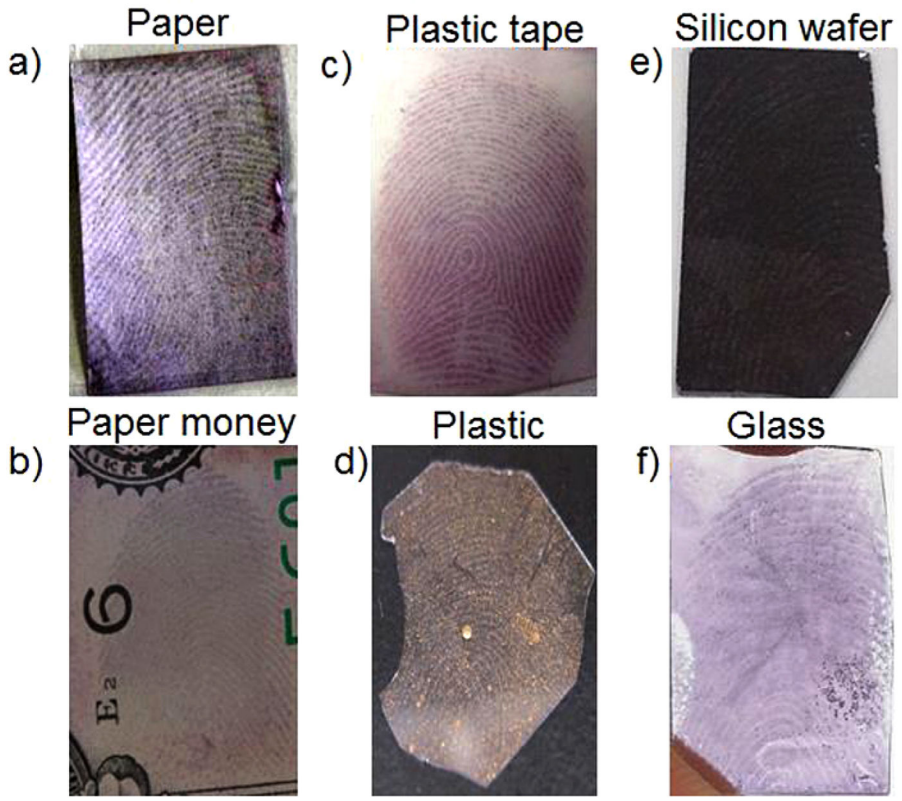

Figure 2.
Colorimetric images of LFPs on three typical different surfaces: (a and b) porous (paper, paper money), (c and d) semiporous (plastic tape, plastic), and (e and f) nonporous (silicon wafer, glass) surfaces.

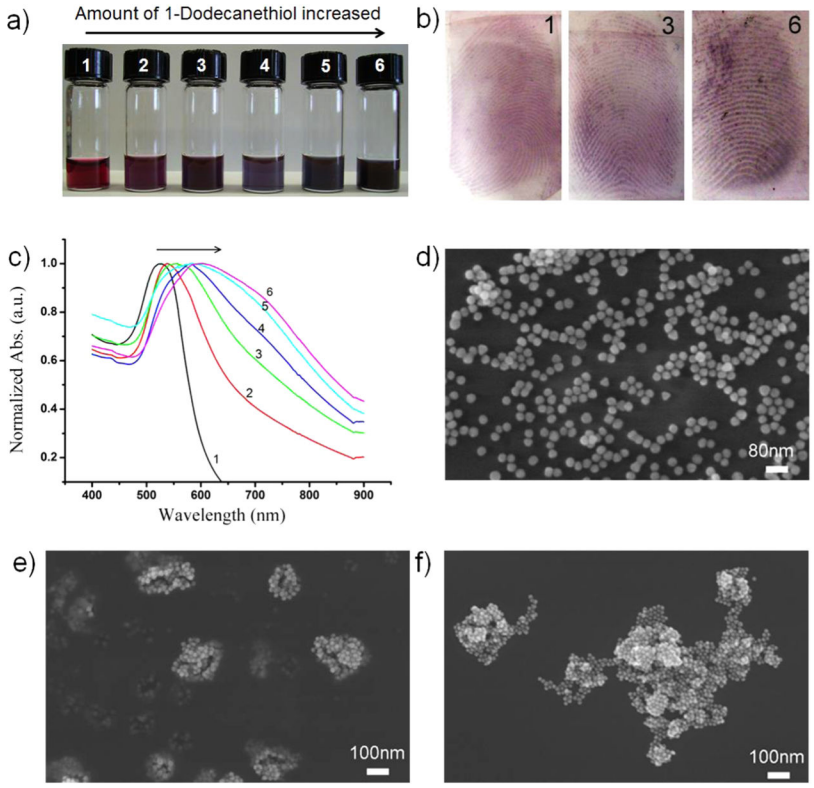

Figure 3.

Self-assembly dependent colorimetric imaging of LFPs using PSMA-*b*-PS functionalized GNPs. (a) Photograph of aqueous solutions of GNPs assembled in the presence of different amounts of 1-dodecanethiol (from 1 to 6: 1, 2, 4, 6, 8, and 10 μL, respectively). (b) Colorimetric images of LFPs using the corresponding 1, 3, and 6 GNPs solutions. (c) UV–vis spectra of aqueous solutions of GNPs at different self-assembly levels (from 1 to 6: 1, 2, 4, 6, 8, and 10 μL, respectively). (d–f) The corresponding SEM images of 1 (d), 2 (e), and 3 (f).

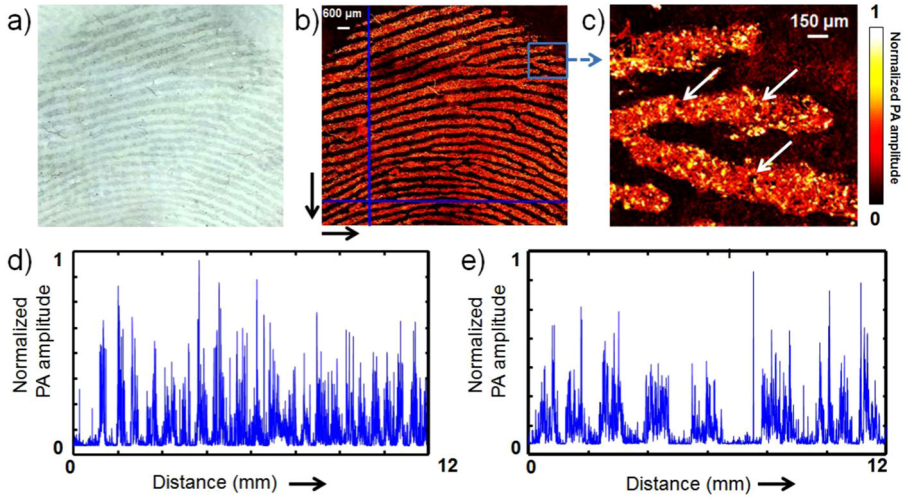

Figure 4.

Photoacoustic imaging of LFPs using PSMA-*b*-PS functionalized GNPs. (a) Bright field image of LFP. (b and c) Photoacoustic images of LFPs. Arrows indicate the pores. (d and e) Normalized photoacoustic amplitudes along with different directions in b: *Y* axis from top to bottom (d) and *X* axis from left to right (e).